

The Pennsylvania State University  
The Graduate School  
College of Earth and Mineral Sciences

**FORECASTING THE NIGHTTIME EVOLUTION OF RADIO WAVE DUCTING  
IN COMPLEX TERRAIN USING THE MM5 NUMERICAL WEATHER MODEL**

A Thesis in  
Meteorology  
by  
Matthew Evan Kucas

Submitted in Partial Fulfillment  
of the Requirements  
for the Degree of

Master of Science

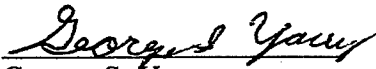
**DISTRIBUTION STATEMENT A**  
Approved for Public Release  
Distribution Unlimited

August 2003


20030929 111

We approve the thesis of Matthew Evan Kucas.

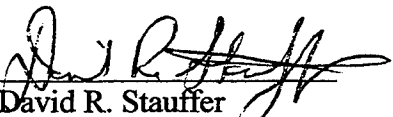
Date of Signature

  
George S. Young  
Professor of Meteorology and  
GeoEnvironmental Engineering  
Thesis Advisor

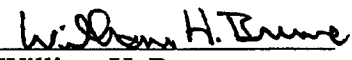
6 June 2003

  
Stephen A. Fast  
Senior Scientist  
Special Signatory

9 June 2003

  
David R. Stauffer  
Senior Research Associate  
Associate Professor of Meteorology

6 June 2003

  
William H. Brune  
Professor of Meteorology  
Head of the Department of Meteorology

6 June 2003

## ABSTRACT

This study tests the effectiveness of using mesoscale models to forecast operationally those atmospheric conditions that cause anomalous propagation of radio waves. Providing early warning about where and when such conditions will develop would be particularly useful for military communications. To test mesoscale models' ability to provide such early warning, the Pennsylvania State University / National Center for Atmospheric Research Fifth Generation Mesoscale Model (MM5) simulates atmospheric conditions around the mountainous, desert terrain near Nellis Air Force Base in Nevada for five forecast periods during the summer and fall of 2002. The extent of ducting regions predicted by the model and the mechanisms that result in the development of those regions are examined. The sensitivity of model predictions to changes in horizontal and vertical resolution is also tested. Results of these analyses reveal that rapid radiational cooling around sunset and subsequent cold air pooling establish vertical temperature gradients that, along with pre-existing moisture gradients, are compacted by gravity waves along the lee sides of mountains within the model domain. This gradient compaction drives changes in the electromagnetic refractivity of the atmosphere that can trap radio waves near the Earth's surface. The sensitivity tests show that increasing the model's horizontal resolution increases the area of predicted ducting significantly. Increasing the vertical resolution does not increase the area of predicted ducting by much, but does sharpen the edges of larger predicted ducting regions.

## Table of Contents

List of Figures	v
List of Tables	vi
Acknowledgements	vii
Introduction	1
Data	4
Procedures	5
Results	10
Discussion	24
References	26

## List of Figures

Fig. 1	Placement of the 18, 6 and 2-km grids over the Nevada test area and terrain within the 2-km grid	7
Fig. 2	Synoptic conditions in and around Nevada.	11
Fig. 3	Extent of predicted ducting in the 2-km grid at 0330 UTC on July 1, 2002.	12
Fig. 4	Potential temperature ( $\theta$ ) contours shown for a prediction period with extensive ducting – July 1, 2002 at 0330 UTC.	14
Fig. 5	Model-derived soundings and ducting predictions across the 2-km domain.	15
Fig. 6	Profiles from the Nellis AFB observation site display the M unit refractivity.	17
Fig. 7	Pre-ducting, ducting and post-ducting model soundings taken from the 2-km domain on July 1, 2002.	19
Fig. 8	Predicted extent of ducting at 0330 UTC on July 1, 2002, for points of common latitude and longitude.	21

---

## List of Tables

Table 1	Number of predicted ducting points at points of common latitude and longitude between the 6 and 2-km domains.	23
---------	---	----

## Acknowledgements

I would first like to thank Dr. George Young and Dr. Stephen Fast for their invaluable support as research advisors and Dr. David Stauffer for answering numerous modeling questions and reviewing this work. I would also like to thank CAPT Michael Gremillion, USAF, for providing the sounding data from Nellis Air Force Base that was used to verify model predictions.

To those who endured a barrage of questions and requests for assistance to address computer issues – Sam Albarano, Rodney Korte, Clark Valentine, Rodney Martin, Tony Schroeder, Brian Reen, Glenn Hunter, Tim Kohler, Tim Fritton and others – I am particularly grateful. And without the support of my family, friends, and my lovely fiancée, Hertta, I would not have had the fortitude to endure the challenges of this research.

Finally, I would like to extend sincere appreciation to the research sponsor, the Oceanographer of the Navy through the program office at the Space and Naval Warfare Systems Command, PM-155. This research was funded by the Naval Sea Systems Command, PMW-155A, contract number N00039-97-D-0042.

## 1. Introduction

Air temperature, vapor pressure, and atmospheric pressure can affect the propagation of electromagnetic radio waves near the surface of the Earth. The following formula describes the relationship between atmospheric variables and radio wave propagation:

$$M = \left(\frac{77.6}{T}\right)\left(p + 4810\frac{e}{T}\right) + 0.157z \quad (1)$$

Here,  $M$  is the modified refractivity in  $M$  units,  $p$  is atmospheric pressure in hectopascals,  $T$  is air temperature in Kelvin,  $e$  is vapor pressure in hectopascals and  $z$  is height above mean sea level in meters (Turton et al. 1988). The formula indicates that refractivity depends more significantly on the amount of moisture in the atmosphere than on either temperature or pressure. Lower temperature and higher vapor pressure yield higher  $M$  values.

Atmospheric temperature and moisture inversions can cause the refractivity near the surface of the Earth to decrease to a minimum value above the surface and then increase above that point. By thus altering the refractivity profile, temperature and moisture inversions can lead to anomalous propagation of radio waves. In extreme cases, the inversions are strong enough to trap a portion of broadcast radio wave energy in a trapping layer near the surface. This trapping layer is called a surface-based duct (Haack and Burk 2001).

Anomalous propagation of radio wave energy due to surface-based ducting is often undesired in areas of military operation. Ducts longer than 100 kilometers that trap



radio wave energy with frequencies at and below radar and communication system frequencies are particularly troublesome. Numerically predicting ducts with these characteristics would provide a distinct operational advantage to military forces in the field.

Recently, mesoscale models have shown a promising ability to predict the atmospheric conditions associated with surface-based ducts (Atkinson et al. 2001; Haack and Burk 2001). Although model forecasts of radio wave ducting are still imperfect due to the limited vertical and horizontal resolution of weather models, it is possible to obtain a qualitative description of the strength and extent of surface-based ducts from these models' forecasts. Many recent numerical modeling studies of atmospheric radio wave ducting have focused on evaporation ducts that form over oceans and seas (Atkinson et al. 2001; Haack and Burk 2001). Numerical models that simulated conditions in these maritime environments have successfully identified mesoscale flow features such as land breezes that are associated with duct development (Atkinson et al. 2001). In turn, these models have characterized the existence and locations of surface-based ducts in the maritime environment, but have produced imperfect predictions of duct height and strength (Atkinson et al. 2001). These inadequacies have resulted from a tendency for mesoscale models to misrepresent the strength of the temperature inversion and the drop in specific humidity across the maritime boundary layer's capping inversion (Haack and Burk 2001). It is reasonable to assume that systematic weaknesses of mesoscale models in forecasting nocturnal flow through mountainous desert terrain could affect numerical ducting predictions in a similar fashion.

Although they do not simulate every detail of small-scale flow accurately, mesoscale models can resolve major land-based atmospheric phenomena that lead to surface-based ducts. Cold air pooling from nocturnal drainage flow in complex desert terrain is one land-based atmospheric phenomenon that affects radio wave propagation. During most evenings, radiational cooling of the desert surface creates temperature gradients along mountain slopes that drive downslope nocturnal drainage flows. Prior research has revealed that these drainage flows are strongest on the shady side of mountains immediately around sunset (Rife et al. 2002). Observations of drainage flows patterns in the Rocky Mountains indicate that widespread drainage flows are more common in the summer and fall than in the winter and spring (Gudiksen et al. 1992). Additionally, the amount of radiational cooling that occurs throughout an evening depends, in part, upon the moisture content of the atmosphere near the surface (Gudiksen et al. 1992). When the atmosphere is drier, outgoing longwave radiation more readily escapes into space, increasing the cooling (Gudiksen et al. 1992).

As with drainage flows, mountain-generated internal gravity waves can affect radio wave propagation (Pelman 2002). The flow of stably-stratified air over complex terrain can generate waves over and downwind of the lee slopes of mountains (Durran and Klemp 1982) and interact with other characteristics of the intermountain flow, such as cold air pooled in leeward valleys. The work that preceded this study demonstrated that mountain waves have a direct effect on duct formation along the lee sides of mountains through the compaction of temperature and moisture gradients (Pelman 2002).

The current study examines the mechanisms that lead to duct development in mountainous desert terrain, the spatial and temporal evolution of duct development, and

the capability of mesoscale models to predict these mechanisms. To accomplish this task, the Penn State / National Center for Atmospheric Research Mesoscale Model version 5 (MM5, Grell et al. 1994) is used to simulate ducting and near-ducting conditions at Nellis Air Force Base in the desert mountains of Nevada for five evenings in the summer and fall of 2002. Observations taken by weather balloons during each of these five evenings indicate ducting or near-ducting conditions.

Model sensitivities to different horizontal and vertical grid resolutions and terrain resolutions are examined. Prior numerical modeling studies of radio wave ducting have used MM5 atmospheric output as input for a radio wave propagation model (Pelman 2002). This research represents another step in the production of an accurate, real-time mesoscale ducting prediction system.

## **2. Data**

Nellis Air Force Base has provided atmospheric soundings for a single time within each test period. The sounding data, with a near-surface vertical resolution of just over thirty meters, serves as forecast verification for MM5 output. The observed soundings from June 25, July 1 and August 2, 2002, indicate the presence of surface-based ducts at the sounding site. Soundings from August 5 and October 11 show near-ducting conditions. MM5 simulations of the three observed ducting periods were used to test the model's capacity to forecast observed ducts. Model simulations of the near-

ducting periods on August 5 and October 11 were used to ensure that it does not over-forecast ducting.

The model initialization did not include raw observations of atmospheric conditions because the availability of such data is often limited in areas of military operation (Haack and Burk 2001). Instead, the Fleet Numerical Meteorology and Oceanography Center's Global Ocean Data Assimilation Experiment (GODAE) provided the Aviation Model (AVN) analysis files used to initialize MM5 model forecasts. These AVN analysis fields have a horizontal resolution of about 0.5 degrees latitude and longitude (NWS 2002). MM5 preprocessing software subsequently interpolated these data to model grid points on a Lambert conformal projection before forecast computing commenced. Each forecast period extended from 0000 UTC to 1200 UTC, with computations beginning at 1200 UTC on the previous day to provide the model sufficient forecast time to adjust variable fields to the mesoscale character of the atmosphere in complex terrain (Haack and Burk 2001). United States Geological Survey databases provided terrain, land use and vegetation data at 5 minute, 2 minute and 30 second resolution for use in the MM5 model predictions.

### **3. Procedures**

The MM5 atmospheric model simulates conditions at and around Nellis Air Force Base for five forecast periods with observed ducting or near ducting conditions: June 25, July 1, August 2, August 5, and October 11, 2002. Each model simulation uses three

nested grids with horizontal resolutions of 18, 6 and 2 kilometers and terrain resolutions of 5 minutes, 2 minutes and 30 seconds respectively (Figure 1). One-way interaction between grids allows coarse grid information to pass into the finer grids boundary conditions at each half hour during the forecast period. One-way grid interaction keeps numerical calculations within coarser grids independent of numerical calculations within finer grids, thus facilitating comparison of predicted surface-based ducting conditions between the 6-km and 2-km grids.

Model runs utilize a standard set of physics parameterizations for each test period. The Gayno-Seaman PBL scheme is chosen for its explicit handling of turbulent kinetic energy and for moist mixing modifications and other updates (Shafran et al. 2000; Stauffer et al. 1999; Stauffer et al. 2001). The 18-km coarse grid model runs employ the Kain-Fritsch cumulus parameterization (Kain and Fritsch 1990), while all three grids use simple ice moist physics (Dudhia 1989). Non-convective nighttime processes were the primary drivers of duct development during each of the test evenings. The Rapid Radiative Transfer Model (RRTM) radiation scheme is selected for its robust handling of long wave radiation processes (Mlawer et al. 1997). A five-layer soil model accounts for diurnal changes in soil temperature (Dudhia 1996).

The MM5 uses a terrain-following, pressure-based vertical coordinate, sigma. Standard model runs for each test period employ 47 sigma levels with about 9 levels in the lowest 400 meters. Prior modeling studies of surface-based radio wave ducting have suggested that high vertical resolution can better resolve the height and extent of ducts (Haack and Burk 2001). To test this finding, high vertical resolution cases for July 1,

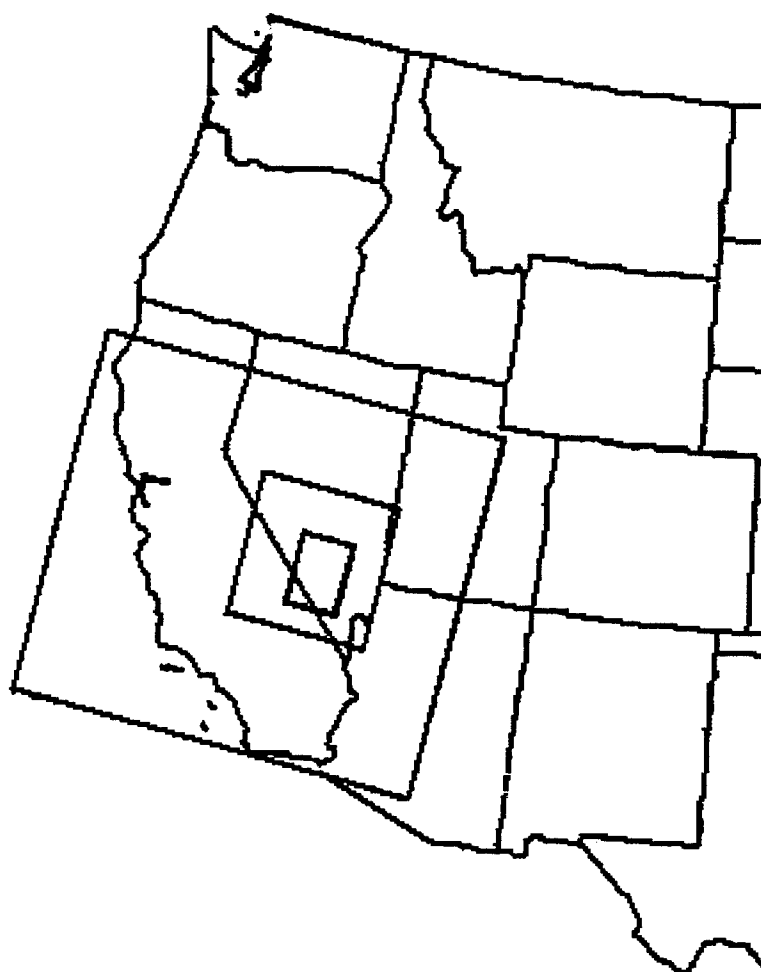


Fig. 1 Placement of the 18, 6 and 2-km grids over the Nevada test area (top) and terrain within the 2-km grid (bottom).

2002 and August 2, 2002, employ 61 sigma levels with about 23 of these packed into the lowest 400 meters. This 61 level setup is used only on the 2-km grid. Thus, the 47 level medium grid output provides the initialization fields and boundary conditions for both the 47 level and 61 level 2-kilometer grid predictions.

Accurate determination of radio wave refractivity profiles requires knowledge about the atmospheric profile in the first several meters above the Earth's surface. However, the first atmospheric model mid-level lies about 10 meters above the surface and the first observation level about 2 meters above the surface. Therefore, Monin-Obukhov (MO) similarity theory fills in missing data between the surface and the first model and observation levels. Refractivity profiles are subsequently derived from both MM5 output and Nellis balloon data in order to check the quality of model predictions. Temperature and specific humidity are derived through the following MO formulae:

$$\theta(z) = \theta_o + \theta_* \left( \frac{\left( \ln \left( \frac{z}{z_o} \right) - \Psi_\theta(\xi) \right)}{k} \right) \quad (2)$$

$$q(z) = q_o + q_* \left( \frac{\left( \ln \left( \frac{z}{z_o} \right) - \Psi_q(\xi) \right)}{k} \right) \quad (3)$$

where  $\theta(z)$  and  $q(z)$  are the potential temperature in Kelvin and the specific humidity in kg/kg at the new height  $z$ ,  $\theta_o$  and  $q_o$  are the potential temperature and the specific humidity at the roughness height  $z_o$ ,  $\theta_*$  is the surface layer potential temperature scale in Kelvin,  $q_*$  is the surface layer moisture scale in kg/kg,  $\Psi_\theta(\xi)$  and  $\Psi_q(\xi)$  are functions that account for atmospheric stability based on height and the Monin-Obukhov length and  $k$  is

the von Karman constant, which has a conventional value of 0.4 (Panofsky and Dutton 1984; Stull 1988). These equations are solved by first assuming neutral stability and thus setting  $\Psi_\theta(\xi)$  and  $\Psi_q(\xi)$  equal to zero. Next, equations 2 and 3 are solved simultaneously for the first two levels above the surface, thus eliminating  $\theta_0$  and  $q_0$  and allowing  $\theta_*$  and  $q_*$  to be explicitly determined. The surface variables  $\theta_0$  and  $q_0$  are not available in the observations and MO-derived values for these surface variables replace model-predicted values to maintain methodological consistency. Calculated values of  $\theta_*$  and  $q_*$  are then used to find the Monin-Obukhov length, and, subsequently, the values of  $\Psi_\theta(\xi)$  and  $\Psi_q(\xi)$ . These new values of  $\Psi_\theta(\xi)$  and  $\Psi_q(\xi)$  yield new  $\theta_*$  and  $q_*$  and the process repeats until  $\theta_*$ ,  $q_*$ ,  $\Psi_\theta(\xi)$  and  $\Psi_q(\xi)$  converge to unchanging solutions. Once these variables have been determined, equations 2 and 3 can be used to calculate  $\theta$ ,  $q$  and, eventually,  $M$  at new heights above ground.

The temporal evolution of meteorological conditions responsible for duct development is examined. Synoptic maps show the large-scale conditions that supported observed ducting on the test evenings. Cross sections of potential temperature and moisture fields from the 2-km model domain output reveal how ducting mechanisms form and decay.

The extent of surface-based ducts across the 6-km and 2-km grids and 2-km grids with different vertical resolutions are also compared to one another. An MM5 post-processing program identifies grid points at which ducting would occur. The number of such ducting points are tabulated and examined qualitatively.



#### 4. Results

June 25, July 1, and August 5, 2002 featured mainly clear skies and very hot temperatures between late afternoon at 0000 UTC and the pre-dawn hours at 1200 UTC. Surface winds were light and southerly throughout each period, ranging from 0-15 knots. Winds at 700hPa (mountain peak level) were southerly to southwesterly at 10-15 knots on June 25 and July 1 and south-southwesterly at 15-30 knots on August 5. October 11, 2002 was also warm, but quite cloudy, with 60 percent to 90 percent cloud cover between 0000 UTC and 1200 UTC (NOAA 2003). Surface winds were southerly to south-southwesterly at 10-15 knots and 700hPa winds were more westerly to south-southwesterly at 25 knots.

August 2, 2002 featured low pressure in Utah and an associated front that entered the 2-km model domain from the northeast. The northern half of the domain was considerably cloudy throughout the 0000 UTC to 1200 UTC period, while the south remained partly cloudy. Surface winds were generally southerly at 0-10 knots. Winds at 700hPa were southeasterly at 10 knots at 0000 UTC and shifted to southwesterly at 5 knots by 1200 UTC. A general overview of synoptic conditions observed in and around Nevada on the test days is given in Figure 2.

Model results indicate a consistent pattern of rapid duct development after sunset both along the synoptic leeside of mountains and in nearby valley floors within the 2-km grid model domain, as shown in Figure 3. Refractivity is quite sensitive to variations in atmospheric moisture content, so a moister surface layer, as observed in sea-based evaporation ducts (Atkinson et al. 2001), can contribute to duct development. Both

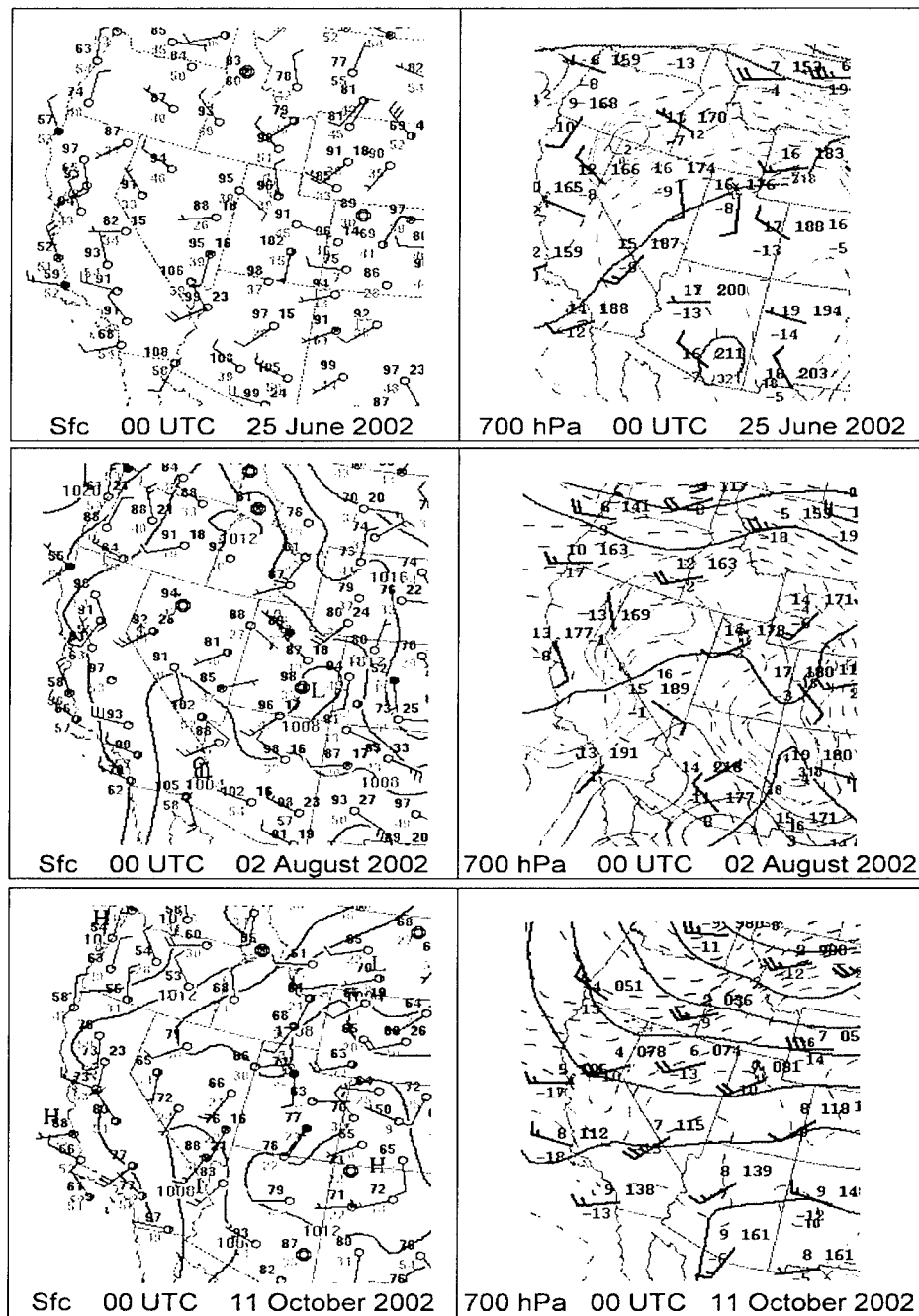


Fig. 2 Synoptic conditions in and around Nevada. Panels from top to bottom show the surface (left) and 700hPa (right) conditions for selected cases: June 25, August 2, and October 11, 2002. The surface maps give temperature, dew point temperature, winds, and pressure contours. The 700hPa maps display temperature, dew point, pressure level heights around a baseline of 3000 meters, pressure level height contours (solid black lines), isotherms (dashed lines) and contours of dew point temperatures above  $-4^{\circ}\text{C}$  (solid green lines). Note the strength and organization of the 700hPa flow on October 11 as compared to the flow on the other two days. (maps provided by the Storm Prediction Center).

Domain 3 terrain + ducts, 0330 UTC Jul 1

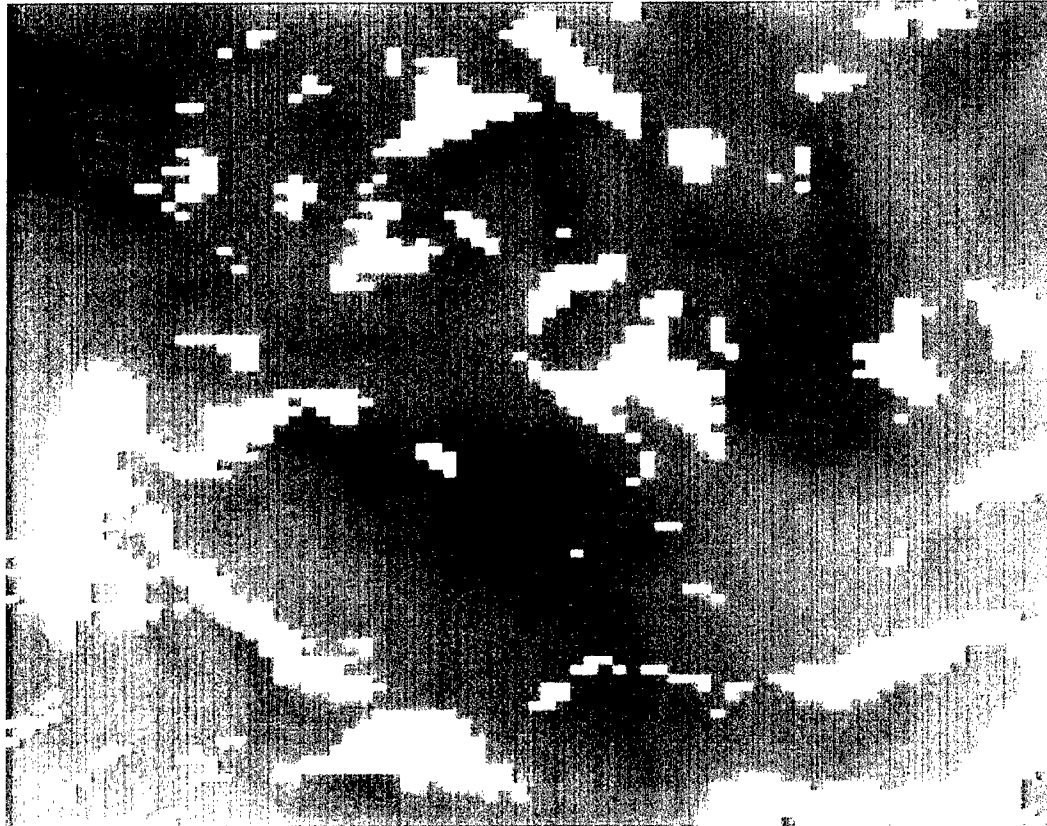


Fig. 3 Extent of predicted ducting in the 2-km grid at 0330 UTC on July 1, 2002. Blue areas represent lower terrain and purple areas higher terrain. Ducts are shaded yellow. Surface and 700hPa winds are generally southerly and leeside ducts are clearly visible along the north, northeast and northwest-facing leeside of mountains in the model domain.

observations and model results, however, indicate only modest moisture content above the surface of the Nevada desert during each of the test evenings. In these cases, radiational cooling in the model domain, facilitated by dry air, drives drainage flow. Cold air subsequently drains down the mountain slopes and pools along the bottoms of the slopes and in the intermountain valleys, establishing a vertical temperature gradient just above the surface. Mountain waves form as the synoptic wind blows over mountain crests in the more stable evening environment, and the waves compress and enhance lee-slope temperature and moisture gradients from above. Compaction of temperature and moisture gradients, as depicted in Figure 4, facilitates anomalous radio wave propagation and, in some cases, surface-based ducting.

The extent of predicted ducting is greatest when mountain waves compress temperature and moisture gradients across large portions of the model domain. Model-predicted ducts are more widespread during the evenings of June 25, July 1 and August 2 than they are during the evenings of August 5 and October 11. As mentioned earlier, observations indicate ducting at the sounding site at 0830 UTC on the three evenings with more extensive predicted ducting, and non-ducting conditions on the two evenings with less extensive predicted ducting. Thus, the soundings consistently support the model's assessment of the favorability of atmospheric conditions for duct development. Figure 5 compares temperature and moisture inversion strength and the predicted extent of ducting at a half an hour past sunset on extensive, moderate and minimal ducting evenings. Model-derived soundings reveal that temperature and moisture inversions near the surface are strongest on the day with the most extensive predicted ducting, July 1, and weakest on the day with the least extensive predicted ducting, October 11.

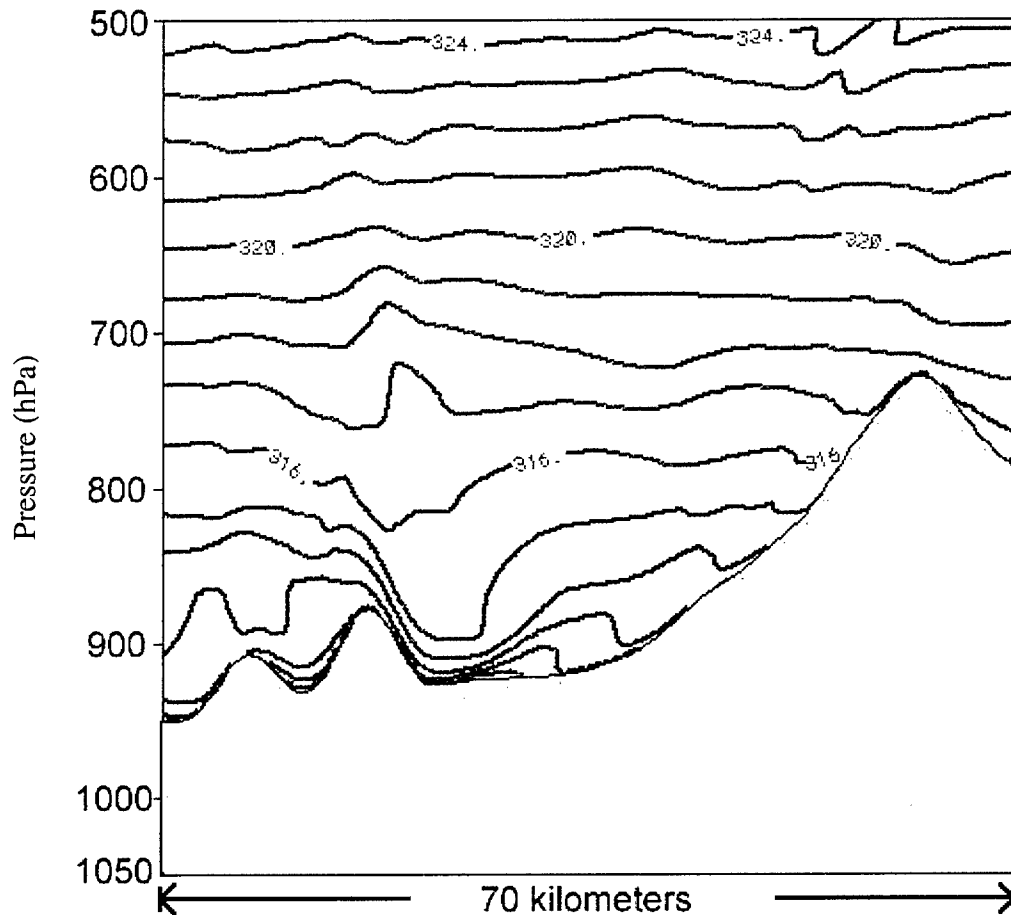


Fig. 4 Potential temperature ( $\theta$ ) contours shown for a prediction period with extensive ducting – July 1, 2002 at 0330 UTC. Note the compaction of the  $\theta$  gradient along the leeside (right) of the middle ridge by a mountain wave and the weakening of the gradient near the center of the valley.

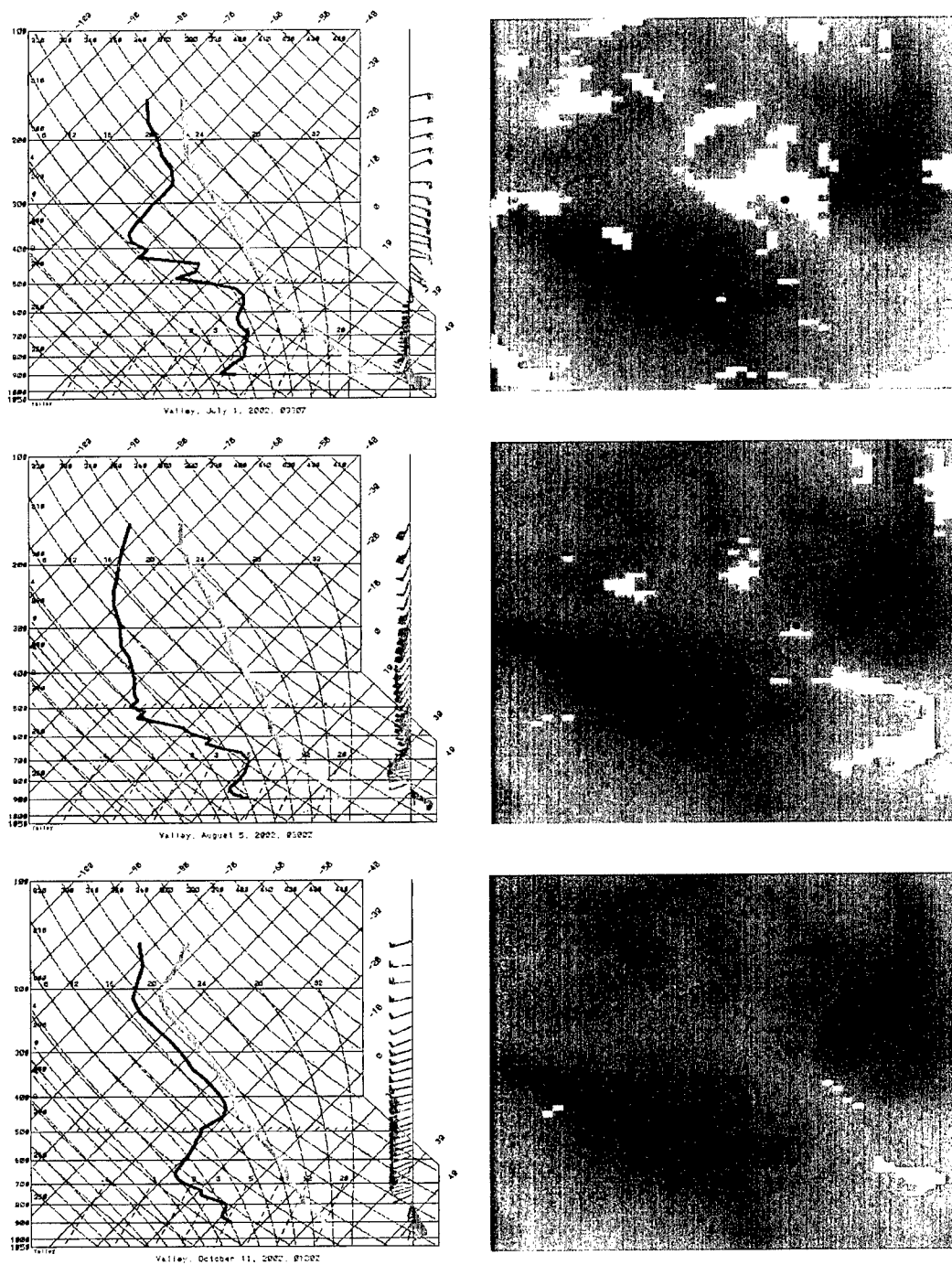


Fig. 5 Model-derived soundings and ducting predictions across the 2-km domain from 0330 UTC, July 1, 2002 (top), 0300 UTC, August 5, 2002 (center), and 0130 UTC, October 11, 2002 (bottom), at peak predicted ducting just after sunset each day. Images on the right display lower terrain in blue, higher terrain in purple and ducts in yellow. A black dot marks the model sounding site.

During most evenings, the synoptic wind blows across the domain from a southerly direction, causing ducts to develop along north, northwest and northeast facing slopes of mountains within the domain. On August 2, another duct development mechanism appears in the 2-km domain. Late in the evening around 0700 UTC, a surface front pushes in from the northeast. Deeper leeside ducts result from elevated temperature and moisture gradients associated with the passing front.

Although test day observations of atmospheric conditions immediately after sunset are unavailable inside the 2-km domain, Nellis AFB has provided observations from 0830 UTC for each period. Figure 6 compares refractivity profiles based on these balloon observations and model output at 0830 UTC. As mentioned earlier, Monin-Obukhov theory is used to fill in missing atmospheric data in the observations below about 2 meters and in the model output below about 10 meters. Refractivity profiles associated with surface-based ducting are visible in the observations on June 25, July 1 and August 2, but not on either August 5 or October 11. Model profiles show weak refractivity inversions around 5 meters above the surface, but these inversions are not strong enough to cause significant ducting conditions. Although refractivity data from model output from the grid point closest to the sounding site do not indicate significant ducting in any of the cases, they do closely follow the refractivity data from the balloon observations, except on October 11. In general, refractivity data from the 2-km grid are slightly closer to observations than data from the 6-km grid near the surface.

The sounding site lies in a shallow valley at the base of the synoptic leeside of a small peak within the 2-km model domain. The underestimation of observed changes in  $dM/dz$  by model predictions may point to a systematic misrepresentation of duct

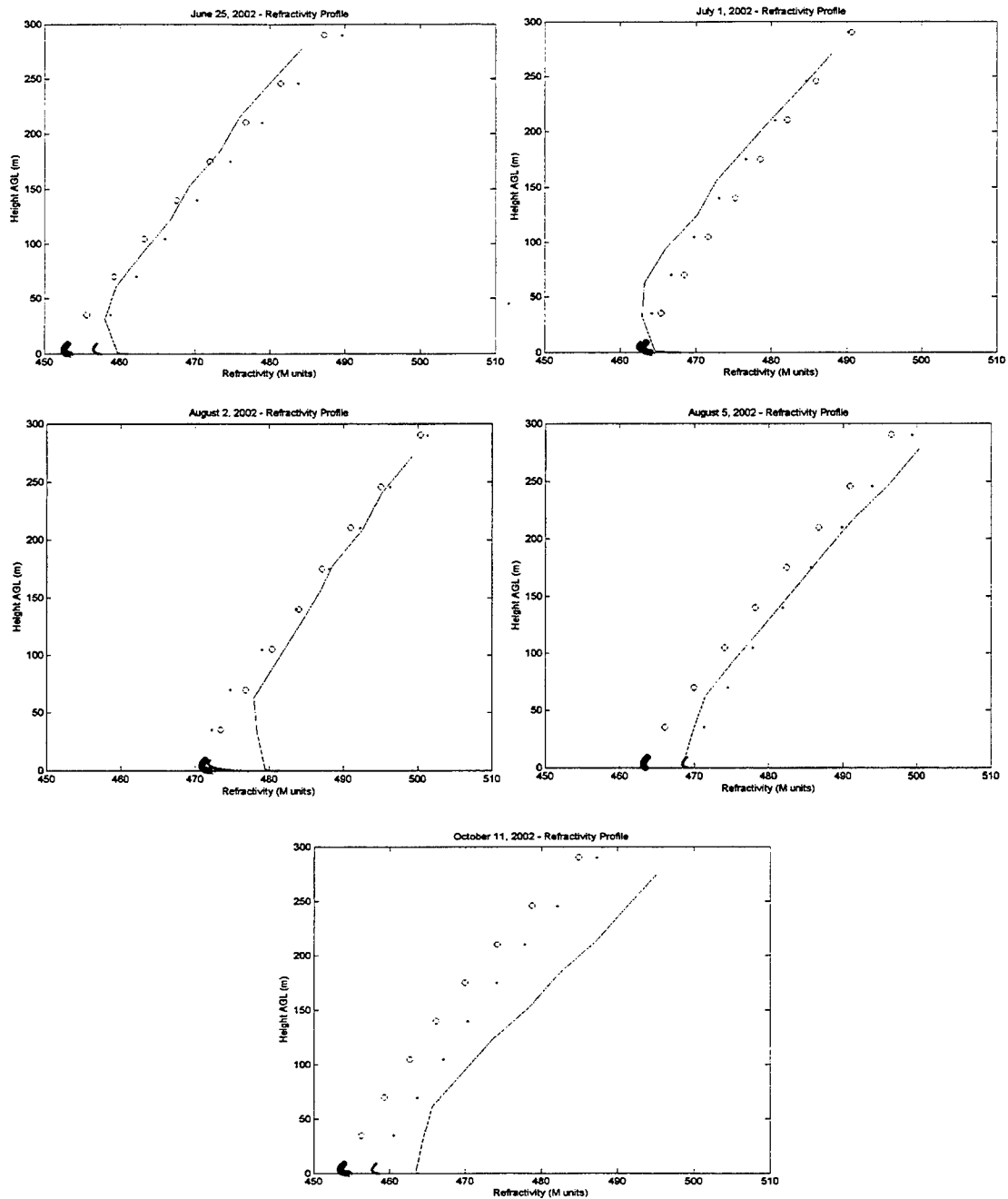


Fig. 6 Profiles from the Nellis AFB observation site display the M unit refractivity for sounding data (solid line), 6-km model domain data (open circles) and 2-km domain data (dots) from 0830 UTC on each test day. Profiles extend from the surface to 300 meters above ground level (AGL). Monin-Obukhov values are visible below 10 meters in the model curves and below 2 meters in the sounding curves. A change in the sign of  $dM/dz$  from negative to positive above the surface in the June 25, July 1 and August 2 observations indicates ducting. Overall, 2-km grid profiles are slightly closer to observation profiles than 6-km grid profiles, particularly near the surface.



coverage and strength across the domain. It is also possible, however, that the model may misrepresent ducting only in shallow valleys adjacent to smaller mountain peaks. In either case, ducts are likely stronger and more extensive in many areas of the domain several hours after sunset than either the 6-km or the 2-km grid forecasts indicate.

Analysis of model output indicates that predicted leeside surface-based ducts are, throughout each forecast period, deepest in the valleys and shallower along the slopes of the mountains. Thus, refractivity inversions do not follow the surface at a uniform height above ground level. Rather, the heights of refractivity inversions correspond to the degree of compaction of temperature and moisture gradients by mountain waves. This compaction occurs closer to the surface near mountain slopes and farther above the surface in the valleys, but not high enough above the valleys to form a duct surface that is level relative to sea level. Thus, ducts are largely, but not completely, terrain following. However, because duct strength – as determined by the lowest frequency of broadcasted radio wave energy a duct will trap - increases non-linearly as a function of duct height, stronger ducts develop in the valleys. Figure 4 shows that the mountain wave compaction effect becomes too weak to support surface-based ducting at some point away from the mountains.

As the evenings progress, temperature and moisture inversions weaken (Figure 7) and the extent of surface-based ducts begins to diminish. Although gradients in temperature and moisture are still present, compression by mountain waves on the leeside of mountains becomes less intense. Ducts tend to lower and weaken from the valley floors inward toward the mountain slopes. This result follows from the evolution of the wavelength of mountain waves during the course of the night. The wavelength of lee

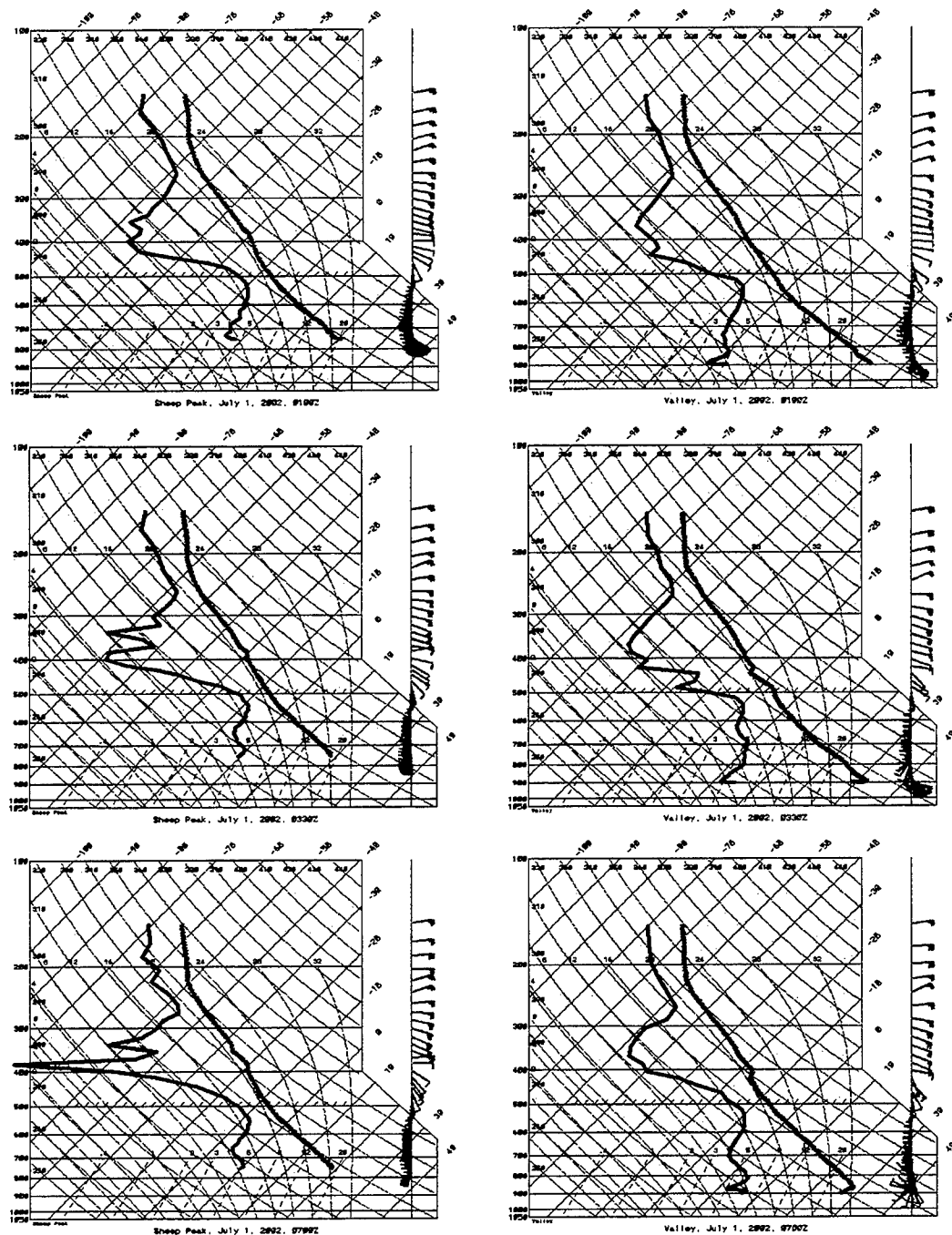


Fig. 7 Pre-ducting (0100 UTC - top), ducting (0330 UTC - center) and post-ducting (0700 UTC - bottom) model soundings taken from the 2-km domain on July 1, 2002. Soundings on the left are taken from the top of a mountain, and soundings on the right are taken from one of the mountain's leeward valleys. All three of the mountain soundings lack the temperature and moisture inversions necessary for duct development. Only the center, valley sounding depicts surface temperature and moisture inversions strong enough to support duct development.

waves depends on the mean synoptic flow,  $U_o$ , and the Brunt-Väisälä frequency,  $N$ , according to the following relationship:

$$\lambda = \frac{U_o}{2\pi N} \quad (4)$$

where  $N$  is:

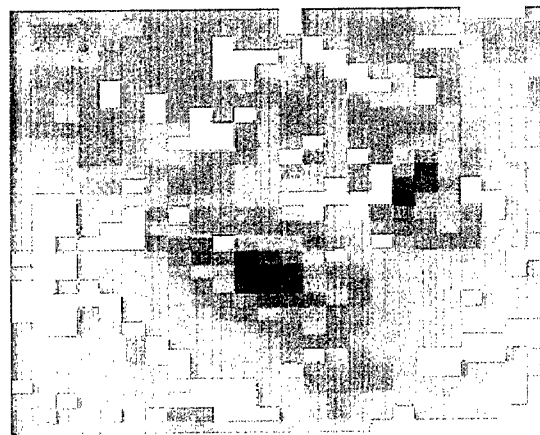
$$N = \left( \frac{g}{\theta_o} \frac{\partial \theta}{\partial z} \right)^{1/2} \quad (5)$$

Throughout widespread ducting periods, the vertical potential temperature gradient increases due to cold air pooling and the mean synoptic wind remains nearly constant. Consequently, the frequency of lee waves increases and the wavelength decreases (Arya 1988). Waves continue to compact gradients, but over a smaller area. Thus, surface-based radio wave ducts are generally more long-lived along the lee slopes of mountains than in the adjacent valleys. If the simulations are correct, extensive anomalous radio wave propagation through most of the intermountain valleys in the model domain should occur only during a few hour period immediately following sunset.

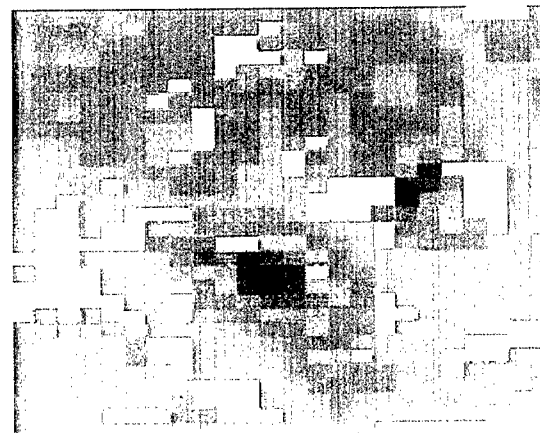
To explore the impact of horizontal resolution, ducting forecasts for grid points of common latitude and longitude (i.e. collocated) within the 6-km and 2-km resolution grids are compared. There are 775 points of common latitude and longitude between the two grids, with 25 such points in the east-west direction and 31 points in the north-south direction. These comparisons, illustrated for the July 1, 2002 case in Figure 8, reveal that increasing model resolution increases the predicted spatial extent of the ducting region. In fact, at these common points, the amount of predicted ducting within the 2-km resolution domain exceeds the amount of predicted ducting within the 6-km



6-km grid  
47 vertical  
levels



2-km grid  
47 vertical  
levels



2-km grid  
61 vertical  
levels

Fig. 8 Predicted extent of ducting at 0330 UTC on July 1, 2002, for points of common latitude and longitude in 6-km grid (top), 2-km grid with 47 vertical levels (center) and 2-km grid with 61 vertical levels (bottom). Lower terrain is shaded blue, higher terrain purple and ducts yellow. Increasing horizontal grid and terrain resolution increases the number of predicted ducting points significantly, but changing the vertical resolution with the 2-km grid does not. However, higher vertical resolution sharpens the edges of large ducting regions and even eliminates some sporadic, local ducting predictions from the lower vertical resolution runs.

resolution domain by about a factor of two for the whole of each test period.

In contrast, the predicted horizontal coverage of surface-based ducts does not differ greatly between the lower and higher vertical resolution model runs for July 1 and August 2. The borders of ducting regions, however, are more sharply defined in the higher vertical resolution runs, as Figure 8 shows. Additionally, duct heights – roughly the levels at which  $dM/dz$  changes sign from negative to positive - predicted by higher vertical resolution runs increase more smoothly between leeward mountain slopes and valley floors.

Table 1 shows the number of ducting points predicted to develop within the 6-km resolution domain and the 2-km resolution domain at points of common latitude and longitude for the entirety of each forecast evening. The values in the table illustrate that predicted ducting is most widespread on the evenings of June 25 and July 1, and becomes less extensive during each of the following forecast evenings.

The predicted extent of large, contiguous ducting areas also differs among the 6-km grid, the 2-km grid with lower vertical resolution and the 2-km grid with higher vertical resolution. The 2-km grid predictions and 6-km grid predictions generally agree upon the location of large ducting regions, but disagree upon the extent of these regions, with much more extensive ducting in the 2-km grid. In contrast, increasing vertical resolution changes the positioning of predicted surface-based ducting regions slightly, but the extent of ducting is nearly the same as in the lower resolution forecast.

	<b>6-km domain</b>	<b>2-km domain</b>	<b>2-km domain (higher res.)</b>
<b>June 25, 2002</b>	564	1239	N/A
<b>July 1, 2002</b>	767	1274	1282
<b>August 2, 2002</b>	310	726	716
<b>August 5, 2002</b>	242	558	N/A
<b>October 11, 2002</b>	51	227	N/A

Table 1 Number of predicted ducting points at points of common latitude and longitude between the 6 and 2-km domains for each of the test periods. Predicted duct extent increases significantly when horizontal grid and terrain resolution increase, but do not change much when vertical resolution increases.

## 5. Discussion

Observations of the atmosphere taken during five nights in the summer and fall of 2002 at Nellis Air Force Base indicate radio wave ducting and near-ducting conditions. Numerical mesoscale weather simulations of these cases show that widespread ducting can occur when mountain waves and cold air pooling work together to produce compact temperature and moisture gradients on the leeside of mountains. Increasing horizontal model resolution and terrain resolution increases aerial coverage of ducting. In contrast, increasing vertical resolution changes the predicted horizontal extent of ducting only slightly and sharpens duct height predictions.

Model output from the 6-km and 2-km domains yield refractivity profiles that closely follow observed refractivity profiles. The model, however, consistently underpredicts abrupt changes in  $dM/dz$  above the desert surface in a shallow valley next to a relatively small mountain within the 2-km domain several hours after sunset. If indicative of a more general trend, these comparisons indicate that the extent of ducting may not drop off as dramatically through the night as model results indicate. More comparisons between model output and observations are, however, necessary before such generalizations can be confirmed.

Future work will determine whether or not changing the amount of vertical diffusion and the boundary layer scheme used by the model will alter the nature and extent of predicted ducting. Further studies will also explore whether predicted ducts are strong enough to trap radio waves at the frequencies mostly commonly used by military

communications equipment. A radio wave propagation model will ingest the MM5 predicted atmospheres to determine precise propagation characteristics.



## References

- Arya, S.P., 1988: *Introduction to micrometeorology*. Academic Press, 303 pp.
- Atkinson, B.W., J.G. Li, and R.S. Plant, 2001: Numerical modeling of the propagation environment in the atmospheric boundary layer over the Persian Gulf. *J. Appl. Meteor.*, **40**, 586-603.
- Dudhia, J., 1989: Numerical study of convection observed during the Winter Monsoon Experiment using a mesoscale two-dimensional model. *J. Atmos. Sci.*, **46**, 3077-3107.
- Dudhia, J., 1996: A multi-layer soil temperature model for MM5, Preprints, *Sixth PSU/NCAR Mesoscale Model Users' Workshop*. 22-24 July 1996, Boulder, Colorado, 49-50.
- Durran, D.R., and J.B. Klemp, 1982: The effects of moisture on trapped mountain lee waves. *J. Atmos. Sci.*, **39**, 2490-2506.
- Grell, G.A., J. Dudhia, and D.R. Stauffer, 1994: A description of the fifth-generation Penn State/NCAR Mesoscale Model (MM5). NCAR Tech. Note 398 1 STR, 122 pp.

- Gudiksen, P.H, J.M. Leone Jr., C.W. King, D. Ruffieux, and W.D. Neff, 1992: Measurements and modeling of the effects of ambient meteorology on nocturnal drainage flows. *J. Appl. Meteor.*, **31**, 1023-1032.
- Haack, T., and S. D. Burk, 2001: Summertime marine refractivity conditions along coastal California. *J. Appl. Meteor.*, **40**, 673-687.
- Kain, J.S., and J. M. Fritsch, 1990: A one-dimensional entraining/detraining plume model and its application in convective parameterization. *J. Atmos. Sci.*, **47**, No. 23, 2784-2802.
- Mlawer, E.J., S.J. Taubman, P.D. Brown, M.J. Iacano, and S.A. Clough, 1997: Radiative transfer for inhomogeneous atmospheres: RRTM a validated correlated-k model for the longwave. *J. Geophys. Res.*, **102**, 16663-16682.
- National Oceanic and Atmospheric Administration (NOAA) Air Resources Lab, cited 2003: Air Resources Lab Ready. [Available online at <http://www.arl.noaa.gov/ready-bin/arlplotafile.pl?metdata=FNL>.]
- National Weather Service (NWS), cited 2003: The GFS atmospheric model. [Available online at <http://wwwt.emc.ncep.noaa.gov/gmb/moorthi/gam.html>.]

Panofsky, H.A., and J.A. Dutton, 1984: *Atmospheric turbulence: models and methods for engineering applications*. John Wiley & Sons, 397 pp.

Pelman, K.S., 2002: An investigation of nocturnal radar ducts that lead to non-line of sight propagation over mountainous terrain., M.S. Thesis, 51 pp. [Available from the Pennsylvania State University.]

Rife, D.L., T.T. Warner, F. Chen, and E.G. Astling, 2002: Mechanisms for diurnal boundary layer circulations in the Great Basin desert. *Mon. Wea. Rev.*, **130**, 921-938.

Shafran, P.C., N.L. Seaman, and G.A. Gayno, 2000: Evaluation of numerical predictions of boundary layer structure during the Lake Michigan Ozone Study. *J. Appl. Meteor.*, **39**, No. 3, 412-426.

Stauffer, D.R., R.C. Munoz and N.L. Seaman, 1999: In-cloud turbulence and explicit microphysics in the MM5. Preprints, *Ninth PSU/NCAR Mesoscale Model Users' Workshop*, Boulder Colorado, 25-25 June, 177-180.

Stauffer, D.R., R.C. Munoz and N.L. Seaman, 2001: On the importance of saturation effects in the turbulence scheme of a mesoscale model. Preprints, *Ninth Conference on Mesoscale Processes*, AMS, Ft. Lauderdale, FL, 30 July - 2 August, 1-5.

Stull, R.B., 1988: *An introduction to boundary layer meteorology*. Kluwer, 666 pp.

Turton, J.D., D.A. Bennetts, and S.F.G. Farmer, 1988: An introduction to radio wave ducting. *Meteor. Mag.*, **117**, 245-254.